Journal of Electroanalytical Chemistry 845 (2019) 126–136

Contents lists available at ScienceDirect

Journal of Electroanalytical Chemistry

journal homepage: www.elsevier.com/locate/jelechem

Mechanism of electrochemical capture of CO_2 via redox cycle of chlorinated 1,4-naphthoquinone in $BMIMBF_4$: An in-situ FT-IR spectroelectrochemical approach

Xuejiao Qiao, Dan Li, Longjiu Cheng, Baokang Jin*

Department of Chemistry, Anhui University, Hefei 230601, People's Republic of China

ARTICLE INFO

Keywords:
CO_2
1,4-Naphthoquinone
2,3-Dichloro-1,4-naphthoquinone
2-Chloro-1,4-naphthoquinone
$BMIMBF_4$
In-situ FT-IR spectroelectrochemistry
Nucleophiles

ABSTRACT

The mechanisms of electrochemical capture of CO_2 via redox cycle of 1,4-naphthoquinone (1,4-NQ), 2,3-dichloro-1,4-naphthoquinone (DCNQ) and 2-chloro-1,4-naphthoquinone (CNQ) in 1-butyl-3-methylimidazolium tetrafluoroborate ($BMIMBF_4$) have been investigated by cyclic voltammetry (CV) and in-situ FT-IR spectroelectrochemistry techniques. In the absence of CO_2, 1,4-NQ and DCNQ undergo a reversible two-step one-electron process while CNQ not. In addition, their two successive electron transfer processes in ionic liquid (IL) are different from that of molecular solvent. There is only a small difference in peak potential between two-step reduction, which possibly due to the ion-pair effects. Meanwhile, the reduction potentials of DCNQ and CNQ shift positively due to the electron-withdrawing effects of chlorine groups. The radical anion ($Q\cdot^-$) and dianion (Q^{2-}) formed during the electrochemical reduction can be used as nucleophiles to attack the eletrophilic carbon center of CO_2 and form a stable CO_2 adduct. For 1,4-NQ, 2 equiv. of CO_2 can be captured during the electrochemical reduction of 1,4-NQ. Whereas, 1 equiv. of CO_2 is captured by 1 equiv. of dianion during the electrochemical reduction of DCNQ and CNQ. Furthermore, CO_2 adducts should be the carbonate type products according to the theoretical calculation results by Gaussian 09 package.

1. Introduction

The excessive CO_2 emission caused by fossil fuel consumption has driven tons of attention to CO_2 separation and reduction [1–5]. Therefore, strategies to decrease the CO_2 emission, such as CO_2 capture, storage, and reduction, have attracted worldwide attention [6–10]. Nucleophiles and alkalines, such as amine, KOH, ammonia, and potassium, are normally used in post-combustion CO_2 capture [11–14]. However, these reagents are limited in practical applications due to their corrosion, energy-intensive to regenerate, easy oxidation, and low CO_2 loading capacity [14]. Therefore, numerous separation approaches, including physical absorption, membranes, ionic liquids, and electrochemical reactions have been employed in CO_2 capture research area [15–18]. Among these new methods, electrochemical reactions, using electrons as strong redox reagents for transformation of target compounds in aqueous or organic solutions, are recognized as a promising way to capture CO_2. Electrochemical methods are more energy-efficient, which can be conducted under relatively mild conditions (20–60 °C) [19].

Quinones and their derivatives, such as 1,4-naphthoquinone (1,4-NQ), 5-hydroxy-1,4-naphthoquinone (HNQ), and p-benzoquinone (BQ), have been widely studied due to their vital roles in electrochemical redox systems [20–23]. Normally, when hydrogen atoms on quinone ring are replaced by electron-withdrawing groups, their electrochemical behavior will also be changed [24]. The radical anion ($Q\cdot^-$) and dianion (Q^{2-}) formed during the electrochemical reduction are good nucleophiles for CO_2 capture, which has attracted lots of attentions, recently [19,24,25]. However, these electrochemical reductions of quinones and their derivatives are usually conducted in buffer solution, aqueous solution and acetonitrile solvent [22,23]. As we all know, how to fix CO_2 in large scale with minimum energy has always been the goal of researchers. Therefore, traditional molecular organic solvents are not favorable option due to their evaporation losses. Ionic liquids, types of molten salts composed of organic cations and organic/inorganic anions, are desirable electrolytes for CO_2 capture due to their negligible vapor pressure, high thermal and electrochemical stability, nonflammability, and high solubility of CO_2 [26–28]. Also, cyclic voltammetric experiments can be readily performed in ionic liquids without supporting electrolyte [29]. Therefore, the application of ionic liquids as electrolytes avoids the use of harsh solvents, catalysts, and

* Corresponding author.
E-mail address: bkjinhf@aliyun.com (B. Jin).

https://doi.org/10.1016/j.jelechem.2019.05.057
Received 31 January 2019; Received in revised form 1 May 2019; Accepted 22 May 2019
Available online 23 May 2019

supporting electrolytes. In addition, $BMIMBF_4$ (1-butyl-3-methylimidazolium tetrafluoroborate) or $BMIMPF_6$ (1-butyl-3-methylimidazolium hexafluorophosphate) type IL is as the most effective and promising of substitute for classical solvents [26,30].

Recently, efforts have been made to electrochemically capture CO_2 in ionic liquids. Hatton has studied the electrochemical capture and release of CO_2 in 1-ethyl-3-methylimizazolium tricyanomethanide ([Emim][TCM]) [19]. The CO_2 electrochemical capture in superbasic [P66614][124Triz] has been studied by Hardacre [31]. The role of anions of 1-butyl-3-methyl-imidazolium ionic liquids during CO_2 electrochemical capture in N-heterocyclic carbene has also been investigated in detail [32]. The electrochemical capture and reduction of CO_2 in ionic liquids gels have been demonstrated by Wallace [33]. Though the electrochemical capture of CO_2 in ionic liquids have been investigated in detail in the past few years, few works related to electrochemical capture of CO_2 in ILs via redox cycle of quinone have ever been presented. Also, the mechanism of CO_2 electrochemical capture and release via redox cycle of quinone and its derivatives in ionic liquids is not clear. Therefore, the stoichiometry of CO_2 electrochemical capture deserves to be further investigated.

It has been demonstrated the advantages of cyclic voltabsorptometry (CVA) and derivative cyclic voltabsorptometry (DCVA) in electrochemical research [34,35]. Therefore, the mechanism of electrochemical capture of CO_2 via redox cycle of 1,4-NQ, DCNQ and CNQ in $BMIMBF_4$ were explored by CV and IR spectroelectrochemistry in this work. The results indicate that electroreduction product can be well used as a nucleophile to capture CO_2. And, the electrochemical capture of CO_2 via redox cycle of chlorinated 1,4-naphthoquinones exhibit different capture mechanisms. In addition, the stoichiometry of CO_2 electrochemical capture was evaluated. Furthermore, combined theoretical computation technique, the possible structure of CO_2 adduct was analyzed.

The structures of 1,4-NQ, DCNQ, CNQ and $BMIMBF_4$ are listed in Scheme 1.

2. Experimental section

2.1. Chemicals

1,4-Naphthoquinone (Sigma–Aldrich, > 98.0%), 2,3-dichloro-1,4-naphthoquinone (Sigma–Aldrich, 98%) and 2-chloro-1,4-naphthoquinone (Sigma–Aldrich, 98%) were used to capture CO_2 during their redox reactions in 1-butyl-3-methylimidazolium tetrafluoroborate ($BMIMBF_4$) (Linzhou Keneng Materials Technology Co. Ltd., 99.99%). High purity carbon dioxide (Nanjing special gas Co. Ltd., 99.99%) is used for electrochemical capture reactions directly. The solution was degassed with high purity nitrogen (Nanjing special gas Co. Ltd., 99.99%) for 10 min before experiment.

2.2. Voltammetry

A three-electrode system with an electrochemical analyzer (Shanghai Chenhua Instrument Co. Ltd., CHI630E potentiostat) was used for electrochemical experiments. A 4 mm diameter gold disk was used as a working electrode. The working electrode was polished with 0.05 μm alumina slurry on a polishing cloth and cleaned with double distilled water and ethanol respectively before experiments. The Ag/AgCl and Pt wire were used as reference electrode and counter electrode, separately.

2.3. In-situ FT-IR spectroelectrochemistry

In-situ FT-IR spectroelectrochemistry experiments were performed in a homemade thin-layer spectroelectrochemical cell [36]. Spectroscopic apparatus (Nicolet Company of the United States, Nicolet iS50) equipped with a specular reflectance accessory and a HgCdTe/A detector cooled with liquid-nitrogen. Each spectrum was composed of 32 interferograms with 0.9 s as sampling intervals. And the spectral resolution was 16 cm^{-1}. The experimental results were processed with Grams/3D software.

2.4. Theoretical computation

The structures were relaxed at the B3LYP [37]/6-311 + + G^{**} level of theory. The energies and NBO (Natural Bond Orbital) charges of the anion radical, dianion were also given at this level of theory. All theoretical calculations were performed by the Gaussian 09 package [38].

3. Results and discussion

3.1. Q in $BMIMBF_4$ without CO_2

The CVs of 1,4-NQ, DCNQ, CNQ in $BMIMBF_4$ are shown in Fig. 1 (recorded at a gold disk electrode, room temperature). There are two unwell-defined couples of anodic and cathodic peaks observed in their electrochemical redox processes. Also, the reduction potential of quinone shifts positively with the increased number of chlorine groups, which is due to the electron-withdrawing effects of chlorine. The two unwell-defined couples of CV peaks are quite different with two well-defined CV waves observed in dimethyl sulfoxide (DMSO), which might be attributed to the ion-pairing effects, especially the interaction between dianion (Q^{2-}) and IL [19,21].

In-situ FT-IR electrochemical experiments were performed in IL. The three-dimensional (3D) spectra are in-situ recorded in the wavenumber range from 1100 cm^{-1} to 1800 cm^{-1} to track the concentration variation of reactant, intermediate and product during the electrochemical reaction (Fig. 2). The downward bands at 1671, 1684 and 1680 cm^{-1} show the concentration of 1,4-NQ, DCNQ and CNQ decrease in the reduction process while recover in the oxidation process. The upward bands at 1370, 1356, and 1408 cm^{-1}, etc. indicate that the concentrations of 1,4-NQ^{2-}, $DCNQ^{2-}$ and CNQ^{2-} increase during the reduction process while decrease during the oxidation process. Specially, the upward bands at 1515, 1510 and 1511 cm^{-1} (assigned to 1,4-NQ $\cdot^{-}$, $DCNQ\cdot^{-}$ and $CNQ\cdot^{-}$ respectively) appear and disappear periodically in both the reduction and oxidation processes [21,22]. During the reduction process, Q is first reduced to $Q\cdot^{-}$ and as the reduction goes on, the intermediate $Q\cdot^{-}$ is reduced to Q^{2-}. Also during the oxidation process, Q^{2-} is oxidized to intermediate $Q\cdot^{-}$ and subsequently $Q\cdot^{-}$ is further oxidized to Q. Therefore, the concentration trend of $Q\cdot^{-}$ in the reduction and oxidation process is similar. The assignment of IR spectra

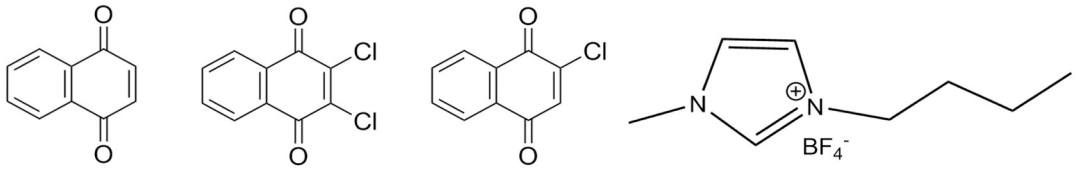

Scheme 1. Structures of 1,4-NQ, DCNQ, CNQ and $BMIMBF_4$.

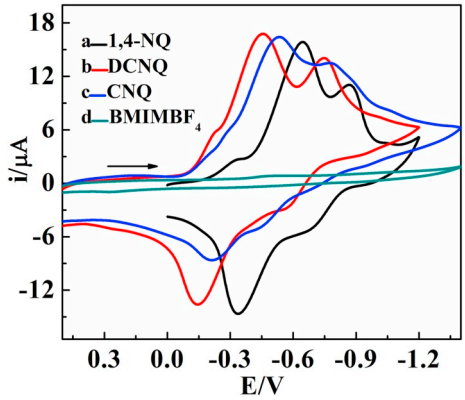

Fig. 1. Cyclic voltammograms in $BMIMBF_4$ containing 20 mmol/L 1,4-NQ (a), DCNQ (b), CNQ (c) and only $BMIMBF_4$ (d), respectively. The potential scan rate was 10 mV/s.

obtained in $BMIMBF_4$ of 1,4-NQ, DCNQ and CNQ are given in Table 1, respectively.

To further explore the electrochemical behavior, the IR spectra are processed to CVA curves (Fig. 3). The absorption bands of Q, $Q^{\cdot -}$ and Q^{2-} increase and decrease periodically with the sweep potential (time). The IR absorption peaks of 1,4-NQ (Fig. 3A) and DCNQ (Fig. 3B) basically return to the initial value at the end of the sweep potential (time). However, IR bands of CNQ does not return to the original state, suggesting that the second step reduction of CNQ in IL is non-reversible, which can also be observed from its CVA curves (Fig. 3C). This non-reversibility was believed to be due to the much stronger interaction of IL with the reduced CNQ than that with the reduced 1,4-NQ and DCNQ as a result of the dipole induced by the ortho-positioned single chlorine group of the reduced CNQ.

DCVA curve is similar to CV wave in ideal state [39]. The DCVA curve greatly suppresses the influence of charging current, which shows two well-defined redox couples of peaks (Fig. 4). The results of DCVA can provide more clear DCVA waveforms when compared with the CV waves in Fig. 1. In addition, the DCVAs at 1515, 1510 and 1511 cm^{-1} correspond to $Q^{\cdot -}$ which have two redox couples of peaks.

The results of CV and IR spectroelectrochemistry indicate that 1,4-NQ and DCNQ undergo a reversible two-step one-electron process (reaction (1) in Scheme 2). While CNQ undergoes a non-reversible two-step one-electron process (reaction (2) in Scheme 2).

3.2. Electrochemical capture of CO_2 via redox cycle of quinone derivatives in $BMIMBF_4$

3.2.1. Electrochemical capture of CO_2 via redox of 1,4-NQ in $BMIMBF_4$

The mechanism of CO_2 capture via electrochemical redox of 1,4-NQ in $BMIMBF_4$ has been investigated by the CV experiments (Fig. 5). As shown in Fig. 5, there is no redox peaks in saturated CO_2 solution without 1,4-NQ when the scan range is 0.7 to −1.6 V (recorded at a gold disk electrode, room temperature). With the addition of CO_2, two reductive waves are merged into one peak. The first reduction peak increases correspondingly, and the current of the single reductive wave C_1 (voltammogram a) is much larger (almost doubled) than that of reductive wave C_3 (voltammogram c). The results indicate that the complexation of CO_2 with the reduced quinone caused the second reduction to shift positively, this positive shift is large enough for both reductions to overlap at the reductive wave C_1. Notably, in voltammogram b, although there is only one reduction peak, two oxidation peaks (A_1 and A_2) are observed. Indeed, with 30% CO_2 in the system, the free reduced 1,4-NQ will exist because there was insufficient CO_2 dissolved in the IL available to react with all of the reduced 1,4-NQ. In the oxidation process, the free reduced 1,4-NQ (Q^{2-}) will be oxidized at A_1 position, so there are two oxidation peaks (A_1 and A_2) in voltammogram b.

To further explore the mechanism of 1,4-NQ with saturated CO_2 in IL, in-situ FT-IR spectroelectrochemistry experiments of 1,4-NQ with saturated CO_2 in IL were performed in a homemade thin-layer [36]. The CV of 1,4-NQ with saturated CO_2 in scan range of 0 to −1.3–0.7 V is shown in Fig. 6A (recorded at a gold disk electrode, room temperature). The corresponding 3D IR spectra presented in Fig. 6B is significantly different from the 3D IR spectra of 1,4-NQ without CO_2 (Fig. 2A). There are only two types of IR absorption bands in Fig. 6B, while the characteristic absorption peak of intermediate-type ($Q^{\cdot -}$) disappears. However, there is a downward band at 2342 cm^{-1} appears, which can be used to track the concentration changes of CO_2. Another new IR absorption peak at 1634 cm^{-1} may be attributed to the product CO_2 adduct.

To further explore the reaction behavior, the IR spectra are processed to CVA curves (Fig. 6C). The absorption bands at 1671, 2342 and 1634 cm^{-1} are used to track the change of 1,4-NQ, CO_2 and $[1,4\text{-NQ-}2CO_2]^{2-}$. The absorbance of 1,4-NQ (1671 cm^{-1}) and CO_2 (2342 cm^{-1}) decrease almost simultaneously in the reduction process, and the variation tendency is the same, indicating that $1,4\text{-NQ}^{\cdot -}$ reacts with CO_2 rapidly to form the initial adduct ($[1,4\text{-NQ-}CO_2]^{\cdot -}$). Subsequently, the $[1,4\text{-NQ-}CO_2]^{\cdot -}$ formed is further reduced and then quickly captures a second equivalent of CO_2. Moreover, the IR absorption bands basically return to the initial value at the end of the sweep potential (time). Consecutive scan results show that the electrochemical capture of CO_2 is a reversible process (see Fig. S1, Supporting information for the details).

The DCVA curves are shown in Fig. 6D, the peak potential of 1671, 2342 and 1634 cm^{-1} is basically the same, which further indicates the rapid chemical reaction between $1,4\text{-NQ}^{\cdot -}$ or $[1,4\text{-NQ-}CO_2]^{2-}$ and CO_2.

The results of CV and IR spectroelectrochemistry indicate that $1,4\text{-NQ}^{\cdot -}$ reacts with CO_2 rapidly to form $[1,4\text{-NQ-}CO_2]^{\cdot -}$ (reactions (3) and (4) in Scheme 3). The IR band at 1515 cm^{-1} (assigned to $1,4\text{-NQ}^{\cdot -}$) disappears due to the chemical reaction of $1,4\text{-NQ}^{\cdot -}$ with CO_2. Subsequently, $[1,4\text{-NQ-}CO_2]^{\cdot -}$ obtains one electron and then captures

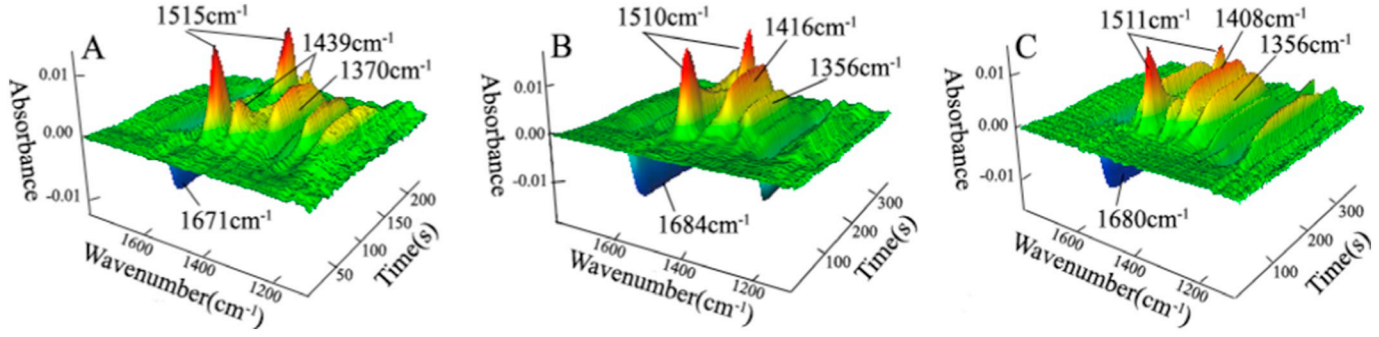

Fig. 2. The corresponding rapid-scan IR spectra in $BMIMBF_4$ of 1,4-NQ (A), DCNQ (B) and CNQ (C), respectively.

Table 1
The assignment of IR absorption bands of 1,4-NQ, DCNQ and CNQ with or without CO_2 [21–23].

1,4-NQ		DCNQ		CNQ	
Wavenumbers (cm^{-1})	Assignment	Wavenumbers (cm^{-1})	Assignment	Wavenumbers (cm^{-1})	Assignment
1671	$\upsilon_{C=O}$ from 1,4-NQ	1684	$\upsilon_{C=O}$ from DCNQ	1680	$\upsilon_{C=O}$ from CNQ
1515	$\upsilon_{C=C}$ from 1,4-NQ$\cdot^-$	1510	$\upsilon_{C=C}$ from DCNQ$\cdot^-$	1511	$\upsilon_{C=C}$ from CNQ$\cdot^-$
1439	$\upsilon_{C=C}$ from 1,4-NQ$\cdot^-$	1416	υ_{C-O} from $DCNQ^{2-}$	1408	υ_{C-O} from CNQ^{2-}
1370	υ_{C-O} from $1,4\text{-}NQ^{2-}$	1356	υ_{C-O} from $DCNQ^{2-}$, $[DCNQ\text{-}CO_2]^{2-}$	1356	υ_{C-O} from CNQ^{2-}, $[CNQ\text{-}CO_2]^{2-}$
2342	$\upsilon_{C=O}$ from CO_2	1640	$\upsilon_{C=O}$ from $[DCNQ\text{-}CO_2]^{2-}$	1636	$\upsilon_{C=O}$ from $[CNQ\text{-}CO_2]^{2-}$
1634	$\upsilon_{C=O}$ from $[1,4\text{-}NQ\text{-}2CO_2]^{2-}$	1387	υ_{C-O} from $[DCNQ\text{-}CO_2]^{2-}$	1386	υ_{C-O} from $[CNQ\text{-}CO_2]^{2-}$
1387	υ_{C-O} from $[1,4\text{-}NQ\text{-}2CO_2]^{2-}$	1320	υ_{C-O} from $[DCNQ\text{-}CO_2]^{2-}$	1317	υ_{C-O} from $[CNQ\text{-}CO_2]^{2-}$
1356	υ_{C-O} from $[1,4\text{-}NQ\text{-}2CO_2]^{2-}$				
1318	υ_{C-O} from $[1,4\text{-}NQ\text{-}2CO_2]^{2-}$				

an additional molecule of CO_2 to yield $[1,4\text{-}NQ\text{-}2CO_2]^{2-}$ (reactions (5) and (6) in Scheme 3). Therefore, the mechanism of electrochemical capture of CO_2 via redox cycle of 1,4-NQ follows the electrochemistry-chemistry-electrochemistry-chemistry (EC_rEC_r) mode. It should be noted that two molecules of CO_2 can be captured during the electrochemical reduction of 1,4-NQ, which will be further discussed in Section 3.3.

3.2.2. Electrochemical capture of CO_2 via redox of DCNQ in $BMIMBF_4$

The CV results of DCNQ with saturated CO_2, unsaturated CO_2 and without CO_2 in IL are shown in Fig. 7 (recorded at a gold disk electrode, room temperature). Two reductive waves can still be observed when saturated CO_2 is introduced (voltammogram a in Fig. 7). It means that DCNQ with CO_2 still requires two reductive waves to form radical anion and dianion, which is obviously different from that of 1,4-NQ with saturated CO_2 (Fig. 5).

However, the CV results obviously show that the second reductive potential of DCNQ with CO_2 becomes more positive and the corresponding oxidative peak is insignificant. In Fig. 7, the second reductive wave shifts positively with the increase of CO_2. However, two reductive waves can still be seen at 100% CO_2 concentration. Moreover, the introduction of CO_2 has no effect on the peak potential of the first reductive wave, indicating that there is no interaction between DCNQ$\cdot^-$ and CO_2.

The IR spectroelectrochemistry experiments of DCNQ with CO_2 were also carried out in order to understand its mechanism. The CV of DCNQ with saturated CO_2 in the scan range of 0.1 to −1.1–0.5 V and the corresponding 3D IR spectra are shown in Fig. 8A and B. Three types of IR bands can still be observed in 3D IR spectra and the upward absorption band at 1510 cm^{-1} (assigned to DCNQ$\cdot^-$) still exists.

In Fig. 8C, the bands at 1684, 2342, 1510, and 1640 cm^{-1} are employed to track DCNQ, CO_2, DCNQ$\cdot^-$, and $[DCNQ\text{-}CO_2]^{2-}$ respectively. In the reduction process, the concentration of DCNQ (1684 cm^{-1}) begins to decrease at about 21 s (−0.11 V). At the same time, the concentration of DCNQ$\cdot^-$ (1510 cm^{-1}) begins to increase at 21 s (−0.11 V), and a maximum concentration is obtained at 72 s (−0.62 V). Subsequently, the DCNQ$\cdot^-$ is further reduced to $DCNQ^{2-}$. $DCNQ^{2-}$ reacts with CO_2 quickly, making the concentration of CO_2 (2342 cm^{-1}) decrease at 60 s (−0.50 V) and reach minimum at 119 s (−1.09 V). Meanwhile, the concentration of $[DCNQ\text{-}CO_2]^{2-}$ (1640 cm^{-1}) begins to increase at 60 s (−0.50 V) and reach maximum at 119 s (−1.09 V). The CVA shows that $DCNQ^{2-}$ reacts with CO_2 (reaction (9) in Scheme 4). And the disappearance of CO_2 (2342 cm^{-1}) obviously lags behind DCNQ (1684 cm^{-1}), which further proves that CO_2 do not participate in the first reduction step of DCNQ. Moreover, the IR absorption bands basically return to the initial value at the end of the sweep potential (time). Consecutive scan results also prove that electrochemical capture of CO_2 via redox of DCNQ is also a chemical reversible process (see Fig. S2, Supporting information for the details).

From Fig. 8D, the shape of DCVA at 1510 cm^{-1} corresponds to DCNQ$\cdot^-$ is similar to that of CV in Fig. 8A. DCVA curves of CO_2 (2342 cm^{-1}) and product (1640 cm^{-1}) correspond to the chemical step, which obviously occurs in the second electrochemical step.

Based on the CV and IR spectral results, DCNQ with CO_2 follows the electrochemistry-electrochemistry-chemistry (EEC_r) mode. The whole reaction process is described in Scheme 4.

3.2.3. Electrochemical capture of CO_2 via redox of CNQ in $BMIMBF_4$

The CV wave of CNQ with saturated CO_2 is shown in Fig. 9A (recorded at a gold disk electrode, room temperature). Compared with Fig. 1c, only one pair of redox waves is observed when saturated CO_2 is introduced. This phenomenon is similar to 1,4-NQ with saturated CO_2. However, the IR absorption band at 1511 cm^{-1} corresponding to the intermediate CNQ$\cdot^-$ still exists (Fig. 9B).

The bands at 1680, 2342, 1511 and 1636 cm^{-1} are selected to track CNQ, CO_2, CNQ$\cdot^-$ and $[CNQ\text{-}CO_2]^{2-}$, respectively (Fig. 9C). In the reduction process, the concentration of CNQ (1680 cm^{-1}) begins to decrease at about 22 s (−0.12 V). Meanwhile the concentration of CNQ

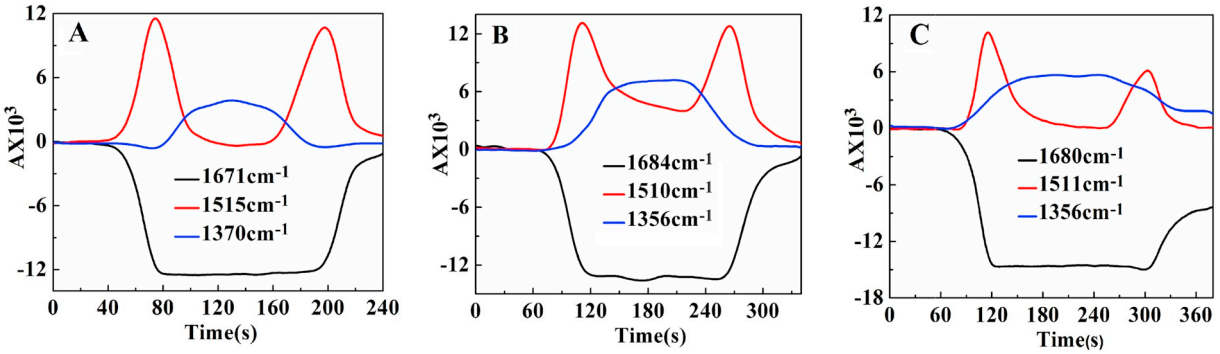

Fig. 3. The corresponding CVAs for 1,4-NQ (A) at 1671, 1515 and 1370 cm^{-1}, for DCNQ (B) at 1684, 1510 and 1356 cm^{-1}, for CNQ (C) at 1680, 1511 and 1356 cm^{-1}, respectively.

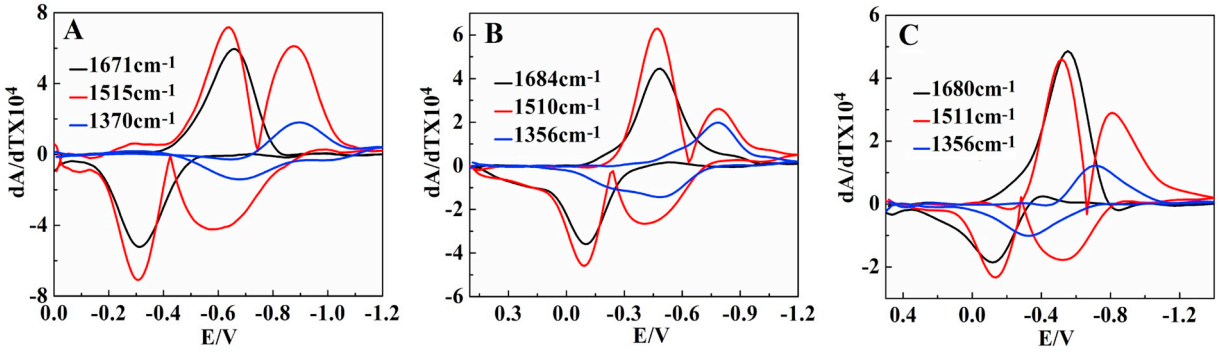

Fig. 4. The corresponding DCVAs for 1,4-NQ (A) at 1671, 1515 and 1370 cm^{-1}, for DCNQ (B) at 1684, 1510 and 1356 cm^{-1}, for CNQ (C) at 1680, 1511 and 1356 cm^{-1}, respectively. To make the DCVA data readily comparable to CV, the DCVA data of 1671, 1684 and 1680 cm^{-1} were multiplied by −1, and 1515, 1510 and 1511 cm^{-1} in the second reduction and the first oxidation were multiplied by −1.

$$Q \overset{e}{\rightleftharpoons} Q^{\cdot -} \overset{e}{\rightleftharpoons} Q^{2-} \quad (1)$$

$$Q \overset{e}{\rightleftharpoons} Q^{\cdot -} \overset{e}{\rightleftharpoons} Q^{2-} \quad (2)$$

Scheme 2. Two-step reduction mechanism of Q.

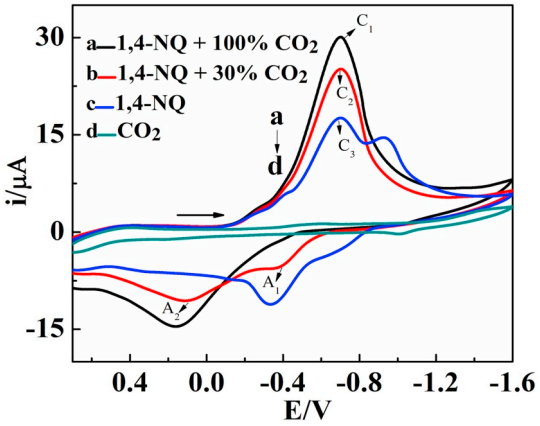

Fig. 5. The CV of containing 20 mmol/L 1,4-NQ with 100% CO_2 (a), with 30% CO_2 (b), only 1,4-NQ (c), only CO_2 (d) in $BMIMBF_4$. Potential scan rate: 10 mV/s.

$\cdot^-$ (1511 cm^{-1}) starts to increase at 22 s (−0.12 V), and a maximum value is obtained at 77 s (−0.67 V). Subsequently, $CNQ\cdot^-$ is further reduced to CNQ^{2-}. Then CNQ^{2-} reacts with CO_2 rapidly, making the concentration of CO_2 (2342 cm^{-1}) decrease at 39 s (−0.29 V) and reach its minimum at 120 s (−1.10 V). At the same time, the concentration of $[CNQ\text{-}CO_2]^{2-}$ (1636 cm^{-1}) begins to increase at 39 s (−0.29 V) and reach its maximum at 120 s (−1.10 V). The results indicate that CO_2 is captured by CNQ^{2-} rather than $CNQ\cdot^-$. In addition, when compared to the CVAs in Fig. 3C, each absorption band in Fig. 9C returns to its original position to a large extent. The reason is that CO_2 captured by CNQ^{2-} is a reversible process (reaction (12) in Scheme 5). So the reversibility of the whole reaction is improved.

It can be clearly seen from Fig. 9D that the DCVA at 1511 cm^{-1} corresponding to $CNQ\cdot^-$ has two redox couples of peaks. Although the CV wave in Fig. 9A has only one pair of redox waves, the DCVA curve at 1511 cm^{-1} corresponds to a two-step one electron transfer process. The results further prove that the dianion CNQ^{2-} reacts with CO_2, rather than the radical anion $CNQ\cdot^-$ and CO_2. In addition, DCVA curves of the absorbance at 2342 cm^{-1} and 1636 cm^{-1} correspond to the chemical step.

The results of CV and IR spectroelectrochemistry show that although CNQ undergoes a non-reversible two-step one electron transfer process in IL, CNQ^{2-} with CO_2 is a reversible chemical reaction. So, its mechanism can be described as electrochemistry-electrochemistry-chemistry (EEC_r) (Scheme 5).

Furthermore, the experiments with different scan rate from 1 to 10 mV/s are also conducted to depict its reaction mechanism (Fig. 10A). With the decrease of scan rate, the second reductive wave begins to appear step wisely. In addition, the CV experiments with different concentration of CO_2 were also performed at a scan rate of 2 mV/s to confirm the reactions between CNQ^{2-} and CO_2 (Fig. 10B). It is clearly shown that the second reduction potential gradually shifts positively with the increase of CO_2 concentration. The results further implied the EEC_r reaction between CNQ and CO_2 (Scheme 5).

3.3. An evaluation of the quantitative relationship on electrochemical capture of CO_2

A series of experiments with different CO_2 mole percent are carried out to explore the stoichiometry of CO_2 capture during the redox reaction of Q in IL. The CVs of 20 mmol/L Q in IL with different concentrations of CO_2 are shown in Fig. 11 (recorded at a gold disk electrode, room temperature). The saturated molarity of CO_2 in $BMIMBF_4$ is defined as 100% mole fraction of CO_2 (≈99 mmol/L) [40,41]; the other percentages are relative concentration of CO_2 with saturated concentration as a reference.

In Fig. 11A, voltammogram j is the CV curve with only CO_2 dissolved in IL, from which it is obvious that the reduction wave appears at about −2.0 V. In fact, with the negative potential scanning, CO_2 may undergo two reactions, that is, CO_2 itself can be further reduced or may combine with the reduced IL [32,42]. Therefore, scanning to the more negative potential, the excess CO_2 is further consumed, whether it is the reduction of CO_2 itself or the capture of CO_2 by the reduced IL. Using this method, the total amount of CO_2 involved in the reaction can be observed, thus further obtaining the stoichiometry of CO_2 capture during the redox reaction of Q.

As can be seen from Fig. 11 that the further reaction of CO_2 does not occur at about −2.0 V when the concentration of CO_2 is low (< 40% in Fig. 11A, < 20% in Fig. 11B, < 20% in Fig. 11C), which indicates that all CO_2 will be completely captured by the reduced Q at lower concentration. However, the further reaction of CO_2 occurs at about −2.0 V when the CO_2 concentration is higher than 30% (> 55% in Fig. 11A, > 30% in Fig. 11B, > 30% in Fig. 11C).

Fig. 12 is the CVAs diagram corresponding to the CV process of Fig. 11. The absorption peak at 2342 cm^{-1} changes obviously when different concentrations of CO_2 are introduced. As for 1,4-NQ, DCNQ and CNQ, at low CO_2 concentration, the absorbance value of 2342 cm^{-1} reaches the minimum at about −1.2 V and remains basically unchanged in the reduction process. The results imply that CO_2 is completely captured by the reduced Q. But, the further reaction of CO_2

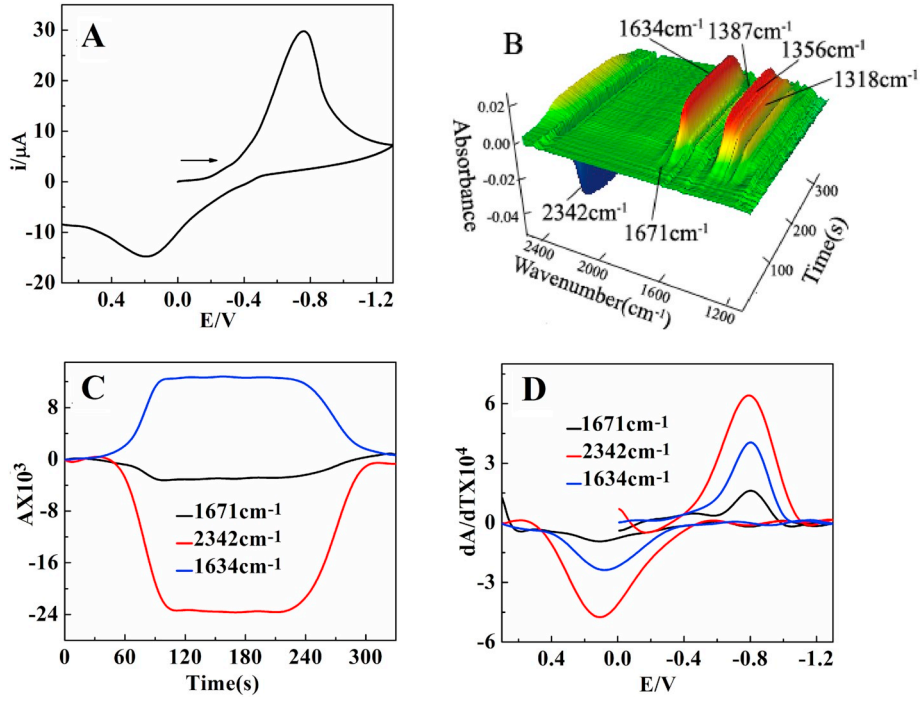

Fig. 6. CV (A) and the corresponding 3D spectra (B) in IL containing 20 mmol/L 1,4-NQ with saturated CO_2. CVA (C) and DCVA (D) of 1,4-NQ with saturated CO_2 at 1671, 2342, 1634 cm^{-1}. To make the DCVA data readily comparable to CV, the DCVA data of 1671 and 2342 cm^{-1} were multiplied by −1.

$$1,4\text{-NQ} + e \rightleftharpoons 1,4\text{-NQ}^{\bullet -} \quad (3)$$

$$1,4\text{-NQ}^{\bullet -} + CO_2 \rightleftharpoons [1,4\text{-NQ-}CO_2]^{\bullet -} \quad (4)$$

$$[1,4\text{-NQ-}CO_2]^{\bullet -} + e \rightleftharpoons [1,4\text{-NQ-}CO_2]^{2-} \quad (5)$$

$$[1,4\text{-NQ-}CO_2]^{2-} + CO_2 \rightleftharpoons [1,4\text{-NQ-}2CO_2]^{2-} \quad (6)$$

Scheme 3. The mechanism of electrochemical capture of CO_2 via redox cycle of 1,4-NQ.

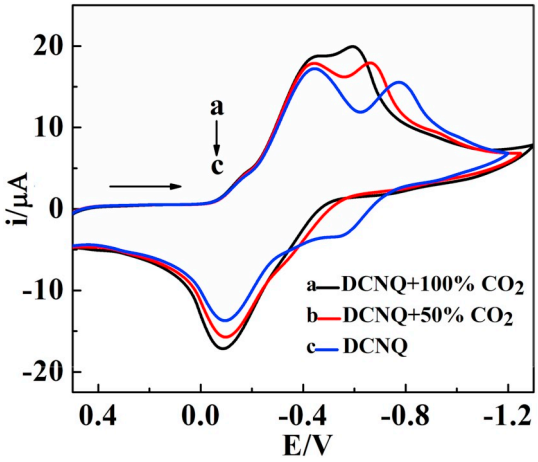

Fig. 7. Reduction of 20 mmol/L DCNQ in $BMIMBF_4$ with 100% CO_2 (a), 50% CO_2 (b) and without CO_2 (c). The potential scan rate was 10 mV/s.

at the more negative potential will be observed when excessive CO_2 is introduced (> 55% in Fig. 12A, > 30% in Fig. 12B, > 30% in Fig. 12C). So, the CVA curves will drop again and reach the minimum value at about −2.4 V (Fig. 12). The CVA curves clearly show the periodic variation of 2342 cm^{-1} in the redox process.

Significantly, the absorbance value of 2342 cm^{-1} at −2.4 V can reflect the total amount of CO_2 involved in the reaction process. From Fig. 13, at −2.4 V, the mole percent of CO_2 (represented by x) and the corresponding absorbance value at 2342 cm^{-1} are in a good linear relationship, respectively. The simulation results further prove that CO_2 participates in the reaction process.

Fig. 14 shows the relationship between CO_2 mole percent and its corresponding absorbance value of IR band at 2342 cm^{-1} at −1.2 V. According to Fig. 14, the corresponding absorbance value decreases dramatically with increase of CO_2 concentrations. However, it decreases slowly at higher CO_2 concentration. At room temperature, the solubility of saturated CO_2 in $BMIMBF_4$ is 99 mmol/L. For 1,4-NQ (Fig. 14A), the intersection of the two lines is at about 40.43% (about 40 mmol/L), which means that 40 mmol/L CO_2 is captured. Therefore, 2 equiv. of CO_2 can be captured during the electrochemical reduction of 1,4-NQ, which is consistent with Scheme 3 proposed. Similarly, the molar ratio between CO_2 and $DCNQ^{2-}$ or CNQ^{2-} is 1:1 (Fig. 14B and C). Therefore, their mechanism can be described in Schemes 4 and 5, respectively.

3.4. Theoretical computation

In order to explore the structure of $[1,4\text{-NQ-}2CO_2]^{2-}$, $[DCNQ\text{-}CO_2]^{2-}$ and $[CNQ\text{-}CO_2]^{2-}$, we make some calculations at the level of B3LYP [37]/6-311++G** with the help of Gauss software. The NBO charges of anion radical ($Q^{\bullet -}$), dianion (Q^{2-}) and the CO_2 adduct ($[1,4\text{-NQ-}CO_2]^{2-}$) were calculated to know which parts possess higher charge densities. Simultaneously, the energies of product were calculated.

In Fig. 15a, for 1.4-$NQ^{\bullet -}$, the NBO charges located at the 1,4-position O-centered and the 2,3-position C-centered are −0.68 and −0.28, respectively. And for $[1,4\text{-NQ-O-}CO_2]^{2-}$ (Fig. 15a), the NBO charges located at the 4-position O-centered and the 3-position C-centered are −0.82 and −0.34, respectively. It is similar to $[1,4\text{-NQ-C-}CO_2]^{2-}$. For $DCNQ^{2-}$ (Fig. 15b), the NBO charges located at the 1,4-position O-centered and the 2,3-position C-centered are −0.80 and − 0.21, respectively. It is similar to CNQ^{2-}. The calculation results

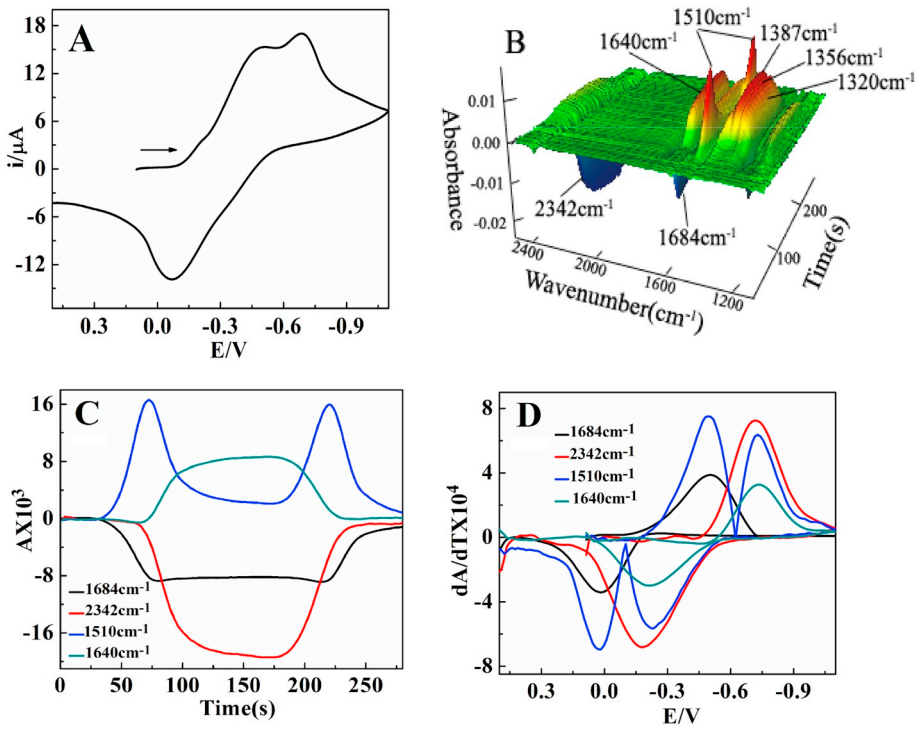

Fig. 8. CV (A) and the corresponding 3D spectra (B) in IL containing 20 mmol/L DCNQ with saturated CO_2; CVA (C) and DCVA (D) of DCNQ with saturated CO_2 at 1684, 2342, 1510, 1640 cm^{-1}. To make the DCVA data readily comparable to CV, the DCVA data of 1684 and 2342 cm^{-1} were multiplied by −1, and 1510 cm^{-1} in the second reduction and the first oxidation were multiplied by −1. The potential scan rate was 10 mV/s.

$$DCNQ + e \rightleftharpoons DCNQ^{\bullet -} \quad (7)$$

$$DCNQ^{\bullet -} + e \rightleftharpoons DCNQ^{2-} \quad (8)$$

$$DCNQ^{2-} + CO_2 \rightleftharpoons [DCNQ\text{-}CO_2]^{2-} \quad (9)$$

Scheme 4. The mechanism of electrochemical capture of CO_2 via redox cycle of DCNQ.

$$CNQ + e \rightleftharpoons CNQ^{\bullet -} \quad (10)$$

$$CNQ^{\bullet -} + e \rightleftharpoons CNQ^{2-} \quad (11)$$

$$CNQ^{2-} + CO_2 \rightleftharpoons [CNQ\text{-}CO_2]^{2-} \quad (12)$$

Scheme 5. The mechanism of electrochemical capture of CO_2 via redox cycle of CNQ.

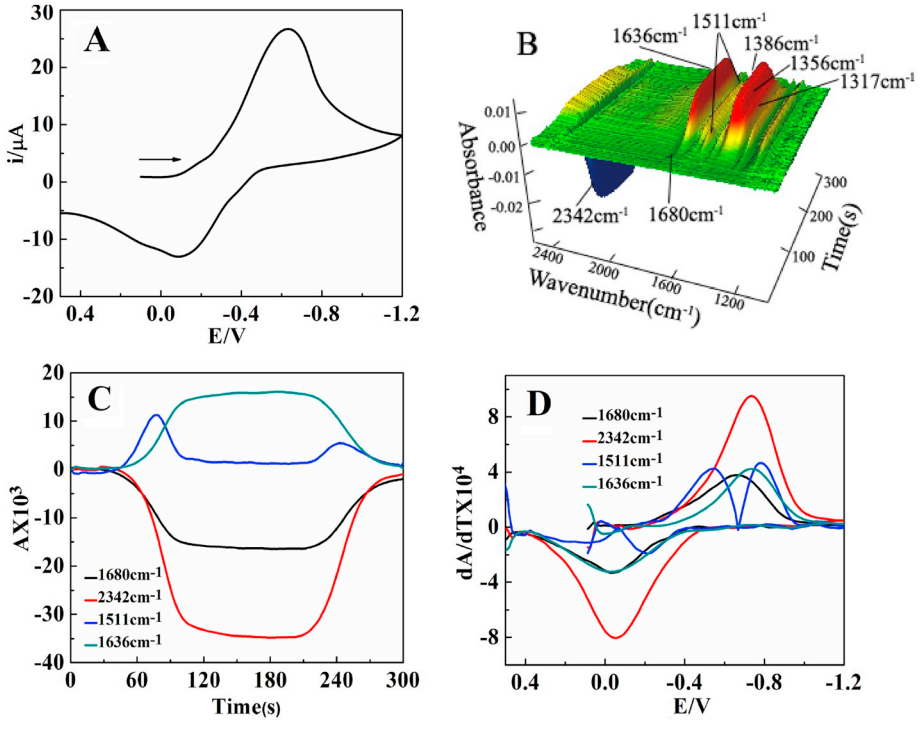

Fig. 9. CV (A) and the corresponding 3D spectra (B) in IL containing 20 mmol/L CNQ with saturated CO_2; CVA (C) and DCVA (D) of CNQ with saturated CO_2 at 1680, 2342, 1511, 1636 cm^{-1}. To make the DCVA data readily comparable to CV, the DCVA data of 1680 and 2342 cm^{-1} were multiplied by −1, and 1511 cm^{-1} in the second reduction and the first oxidation were multiplied by −1. The potential scan rate was 10 mV/s.

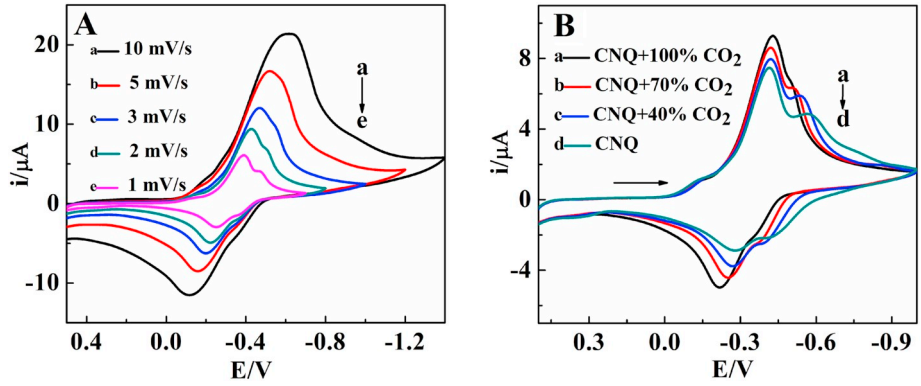

Fig. 10. Cyclic voltammograms at various scanning rates in IL containing 20 mmol/L CNQ with saturated CO_2 (A). The CV of 20 mmol/L CNQ in IL with 100% CO_2 (a), 70% CO_2 (b), 40% CO_2 (c) and without CO_2 (d) (B). The potential scan rate was 2 mV/s.

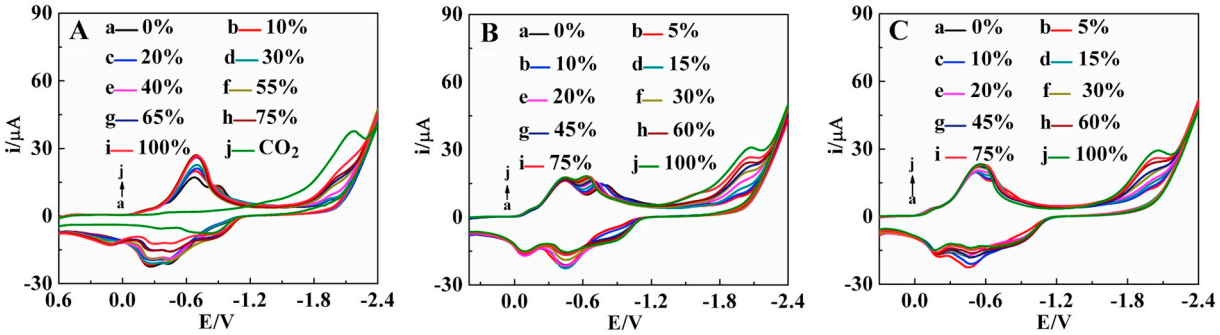

Fig. 11. The CV of 20 mmol/L 1,4-NQ (A), DCNQ (B) and CNQ (C) in IL with different CO_2 mole percent respectively. The potential scan rate was 10 mV/s.

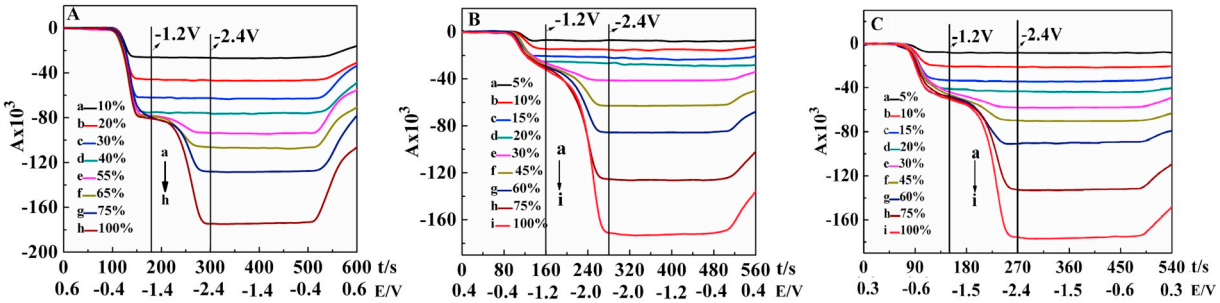

Fig. 12. The CVAs of 20 mmol/L 1,4-NQ (A), DCNQ (B) and CNQ (C) in IL with different CO_2 mole percent, respectively.

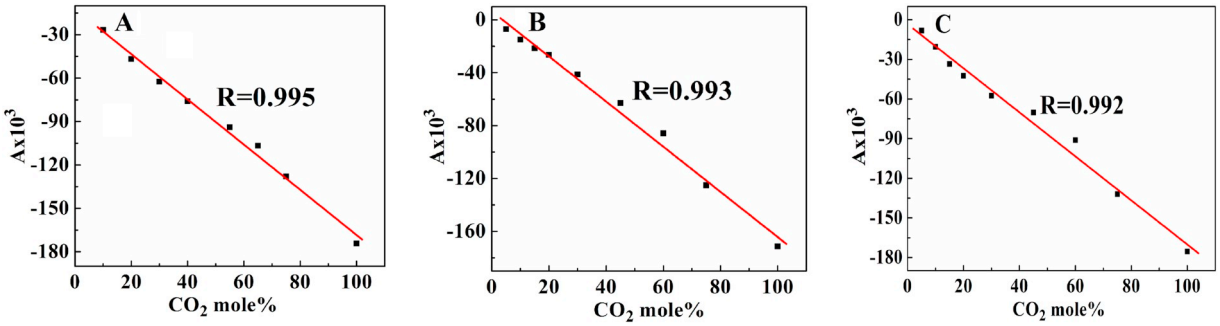

Fig. 13. A-x diagram of 20 mmol/L 1,4-NQ (A), DCNQ (B) and CNQ (C) in IL with different CO_2 mole percent at −2.4 V, respectively.

show that O-centered has more electron localization and stronger nucleophilicity than C-centered.

In addition, CO_2 reacts with 1,4-NQ$\cdot^-$ instead of DCNQ$\cdot^-$ or CNQ$\cdot^-$. The reason maybe the electron-withdrawing effects of chlorine group, which making the charge densities of DCNQ or CNQ smaller. So the nucleophilicity of DCNQ$\cdot^-$ or CNQ$\cdot^-$ gets lower and it is difficult to attack the C-centered of CO_2. For this reason, the charges of DCNQ$\cdot^-$ and CNQ$\cdot^-$ are calculated (Fig. 15c). Compared the charges of 1.4-NQ$\cdot^-$, DCNQ$\cdot^-$ with CNQ$\cdot^-$, obviously 1,4-NQ$\cdot^-$ has higher charge densities.

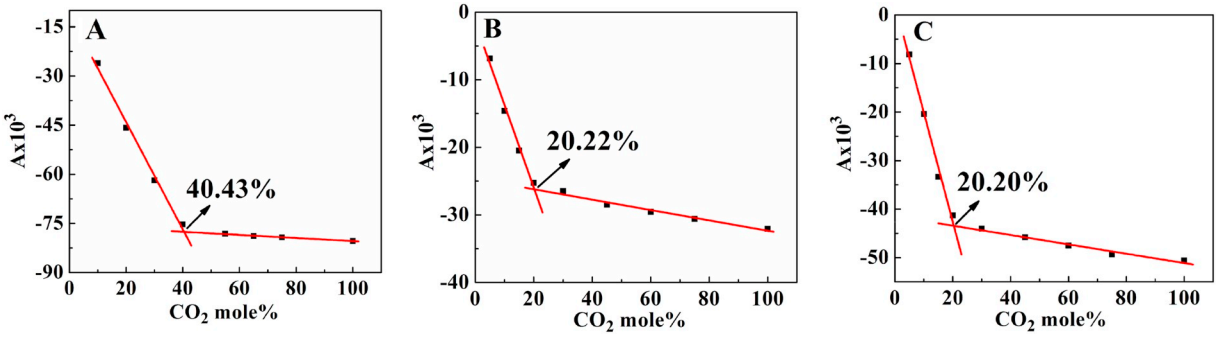

Fig. 14. A-x diagram of 20 mmol/L 1,4-NQ (A), DCNQ (B) and CNQ (C) in IL with different CO_2 mole percent at −1.2 V, respectively.

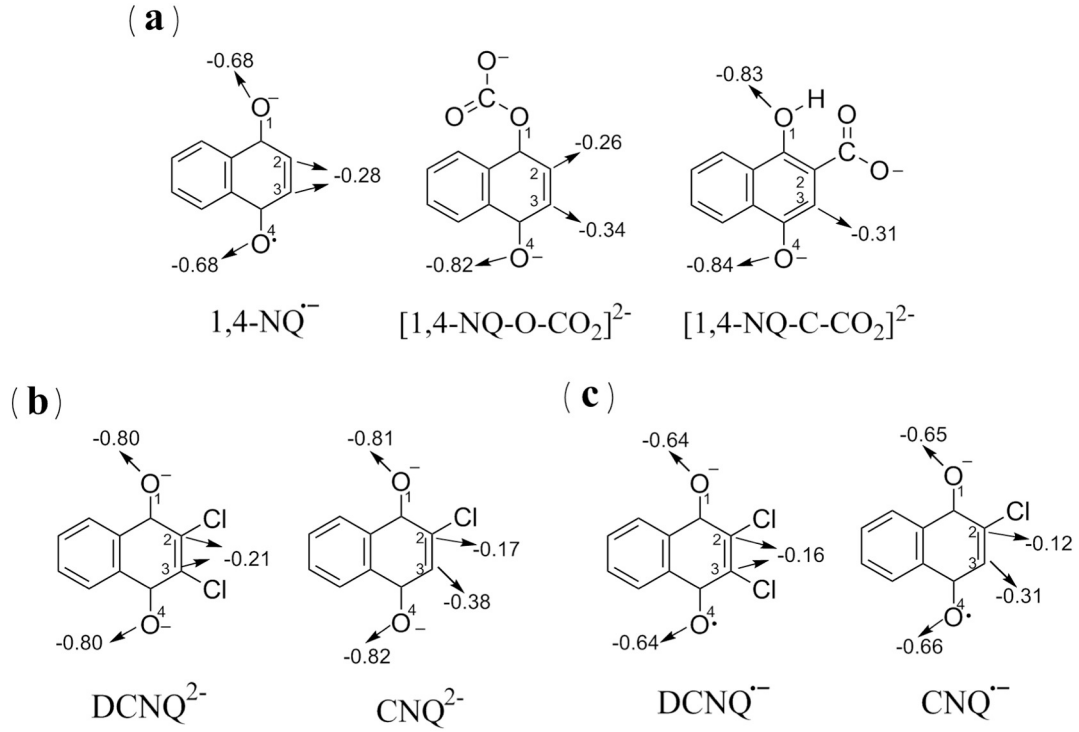

Fig. 15. The values of NBO charges for the anion radical, dianion and the CO_2 adduct were given at B3LYP/6-311++G** level.

Subsequently, the energies of product are calculated and the results are listed in Fig. 16. For 1,4-NQ, for its initial adduct $[1,4\text{-NQ-CO}_2]\cdot^-$ (Fig. 16a1), the calculation results show that carbonate adduct $[1,4\text{-NQ-O-CO}_2]\cdot^-$ is 0.20 eV higher than carboxylate adduct $[1,4\text{-NQ-C-CO}_2]\cdot^-$. The results of energy calculation are similar to the calculation results of $[BQ\text{-CO}_2]\cdot^-$ [24]. And for the product $[1,4\text{-NQ-2CO}_2]^{2-}$ (Fig. 16a2), the results of energy calculation show that carbonate-carboxylate type adduct ($[1,4\text{-NQ-O-C-2CO}_2]^{2-}$) has the lowest energy. Although the results of energy calculation which show carbonate-carboxylate type adduct $[1,4\text{-NQ-O-C-2CO}_2]^{2-}$ is more stable than bis(carbonate) adduct $[1,4\text{-NQ-O-O-2CO}_2]^{2-}$ adduct, bis(carbonate) adduct is reported as the product in the literature [19]. In addition, the chemical reaction of the electroreduction product with CO_2 is a nucleophilic reaction, so from the results of the NBO charge calculation (Fig. 15a), it can be speculated that its reaction mechanism may follow the EC_rEC_r mode of the reaction (13) in Scheme 6 more reasonably.

For CNQ (Fig. 16b), carbonate adduct ($[CNQ\text{-O-CO}_2]^{2-}$) is 0.23 eV lower than carboxylate adduct ($[CNQ\text{-C-CO}_2]^{2-}$). Whereas for DCNQ (Fig. 16c), from the perspective of reversibility of the whole reaction, the chlorine atom cannot be replaced by CO_2. Therefore, it is impossible to produce carboxylate product ($[DCNQ\text{-C-CO}_2]^{2-}$), and carbonate product ($[DCNQ\text{-O-CO}_2]^{2-}$) is more reasonable.

The calculation results indicate that the CO_2 adduct should be carbonate-type structure. Therefore, their mechanisms can be elaborated in Scheme 6. In fact, carbonate-type product has also been reported as the main product [19,24,43].

4. Conclusions

In summary, CV and IR spectroelectrochemistry techniques were used to investigate the mechanism of electrochemical capture of CO_2 via redox cycle of 1,4-NQ, DCNQ and CNQ in $BMIMBF_4$, respectively. Our research shows that chlorine group plays an important role in electrochemical capture of CO_2 via redox cycle of quinones.

The redox mechanisms of 1,4-NQ and DCNQ in IL both follow the reversible EE mode, while CNQ follows the non-reversible EE mode.

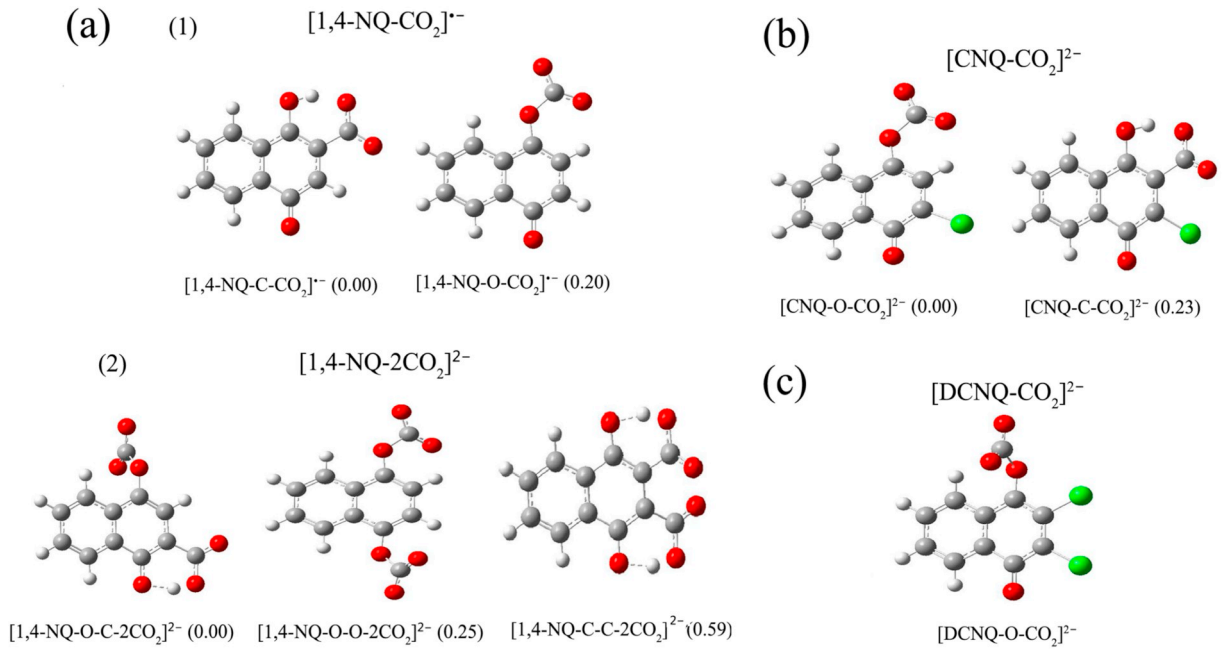

Fig. 16. The energies for the possible structure of CO_2 adduct were calculated at the B3LYP/6-311 + +G** level of theory. The value in the brackets was relative energy in e*V*.

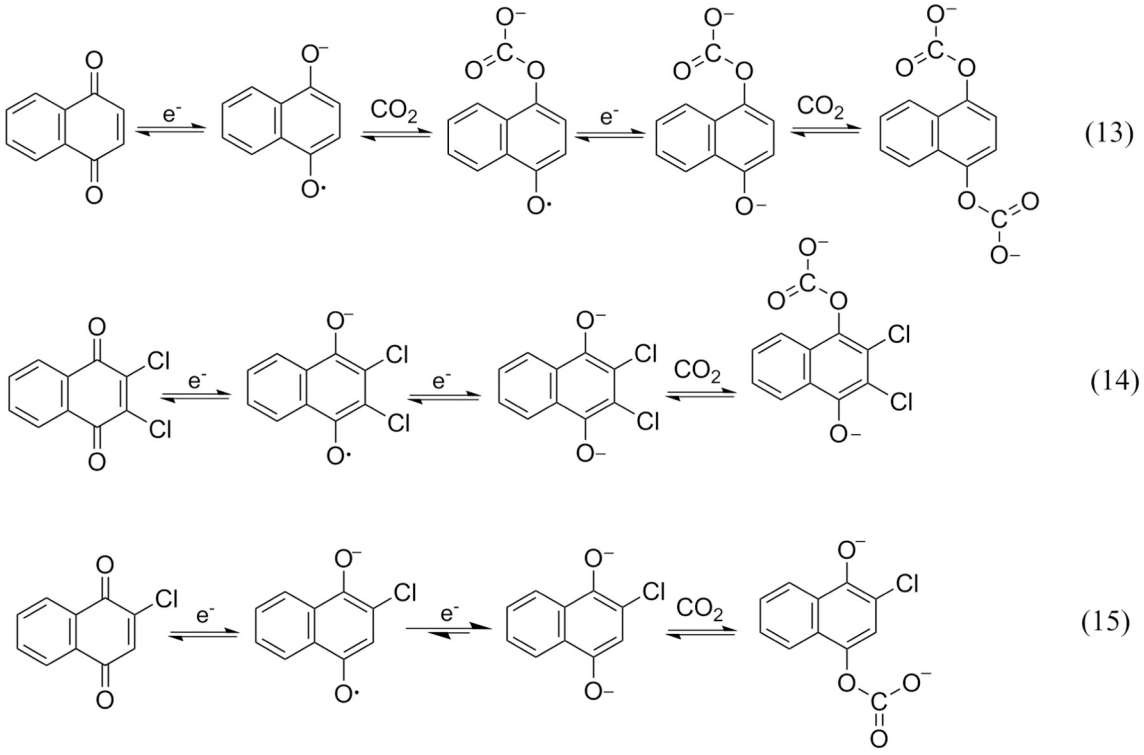

Scheme 6. The mechanism of electrochemical capture of CO_2 via redox cycle of 1,4-NQ (13), DCNQ (14), CNQ (15), respectively.

However, in the presence of CO_2, 1,4-NQ, DCNQ and CNQ follow the modes of EC_rEC_r, EEC_r and EEC_r, respectively. The results show that the reduced quinones can be well used as nucleophiles to capture CO_2. Quantitatively, it is found that both the molar ratio between CO_2 and 1.4-NQ$\cdot^-$ or $[1,4\text{-NQ-}CO_2]^{2-}$ is 1:1; whereas the molar ratio of CO_2 and $DCNQ^{2-}$ or CNQ^{2-} is 1:1. CO_2 adduct should be carbonate-type products according to the theoretical calculation results. In addition, CO_2 can be released during the redox cycle of quinones since the chemical reaction of the electroreduction product with CO_2 is reversible. Therefore, 1,4-NQ, DCNQ and CNQ are promising adsorbents, which can be regenerated easily.

Acknowledgment

This work has been supported by the National Natural Science Foundation of China (Grants 21175001 and 21375001).

Appendix A. Supplementary data

Supplementary data to this article can be found online at https://doi.org/10.1016/j.jelechem.2019.05.057.

References

[1] X.F. Cui, J. Wang, B. Liu, S. Ling, R. Long, Y.J. Xiong, Turning au nanoclusters catalytically active for visible-light-driven CO_2 reduction through bridging ligands, J. Am. Chem. Soc. 140 (2018) 16514.

[2] D.R. Kauffman, D.R. Alfonso, D. Tafen, C.J. Wang, Y.Y. Zhou, Y. Yu, J.W. Lekse, X.Y. Deng, V. Espinoza, J. Trindell, O.K. Ranasingha, A. Roy, J.S. Lee, H.L.L. Xin, Selective electrocatalytic reduction of CO_2 into CO at small, thiol-capped Au/Cu nanoparticles, J. Phys. Chem. C 122 (2018) 27991.

[3] S. Nadeem, A. Mumtaz, M. Mumtaz, M.I.A. Mutalib, M.S. Shaharun, B. Abdullah, Visible light driven CO_2 reduction to methanol by Cu-porphyrin impregnated mesoporous Ti-MCM-48, J. Mol. Liq. 272 (2018) 656.

[4] Y. Osaka, T. Tsujiguchi, A. Kodama, Experimental investigation on the CO_2 separation performance from humid flue gas by TSA process, Sep. Purif. Technol. 207 (2018) 77.

[5] D.B. Shinde, M. Ostwal, X.B. Wang, A.M. Hengne, Y. Liu, G. Sheng, K.W. Huang, Z.P. Lai, Chlorine-functionalized keto-enamine-based covalent organic frameworks for CO_2 separation and capture, Crystengcomm 20 (2018).

[6] Y.X. Ge, H. Zhou, Y.J. Ji, L.F. Ding, Y.Y. Cheng, R.Y. Wan, S.Y. Yang, Y.F. Liu, X.Y. Wu, Y.Y. Li, Understanding water adsorption and the impact on CO_2 capture in chemically stable covalent organic frameworks, J. Phys. Chem. C 122 (2018) 27495.

[7] G.P. Hammond, S.S.O. Akwe, S. Williams, Techno-economic appraisal of fossil-fuelled power generation systems with carbon dioxide capture and storage, Energy 36 (2011) 975.

[8] Y. He, F. Wang, Hydrate-based CO_2 capture: kinetic improvement via graphene-carried $-SO_3^-$ and Ag nanoparticles, J. Mater. Chem. A 6 (2018) 22619.

[9] R. Hegner, L.F.M. Rosa, F. Harnisch, Electrochemical CO_2 reduction to formate at indium electrodes with high efficiency and selectivity in pH neutral electrolytes, Appl. Catal. B Environ. 238 (2018) 546.

[10] D. Li, H. Furukawa, H.X. Deng, C. Liu, O.M. Yaghi, D.S. Eisenberg, Designed amyloid fibers as materials for selective carbon dioxide capture, Proc. Natl. Acad. Sci. U. S. A. 111 (2014) 191.

[11] T.N.G. Borhani, A. Azarpour, V. Akbari, S.R.W. Alwi, Z.A. Manan, CO_2 capture with potassium carbonate solutions: a state-of-the-art review, Int. J. Greenhouse Gas Control 41 (2015) 142.

[12] S. Dharmalingam, K.T. Park, J.Y. Lee, I.G. Park, S.K. Jeong, Catalytic effect of metal oxides on CO_2 absorption in an aqueous potassium salt of lysine, J. Ind. Eng. Chem. 68 (2018) 335.

[13] L.M.C. Pereira, L.F. Vega, A systematic approach for the thermodynamic modelling of CO_2-amine absorption process using molecular-based models, Appl. Energ. 232 (2018) 273.

[14] B.T. Zhao, Y.X. Su, W.W. Tao, L.L. Li, Y.C. Peng, Post-combustion CO_2 capture by aqueous ammonia: a state-of-the-art review, Int. J. Greenhouse Gas Control 9 (2012) 355.

[15] M.Z. Ahmad, V. Martin-Gil, V. Perfilov, P. Sysel, V. Fila, Investigation of a new co-polyimide, 6FDA-bisP and its ZIF-8 mixed matrix membranes for CO_2/CH_4 separation, Sep. Purif. Technol. 207 (2018) 523.

[16] C.A. Daly, T. Brinzer, C. Allison, S. Garrett-Roe, S.A. Corcelli, Enthalpic driving force for the selective absorption of CO_2 by an ionic liquid, J. Phys. Chem. Lett. 9 (2018) 1393.

[17] A. Yokozeki, M.B. Shiflett, C.P. Junk, L.M. Grieco, T. Foo, Physical and chemical absorptions of carbon dioxide in room-temperature ionic liquids, J. Phys. Chem. B. 112 (2008) 16654.

[18] Y.P. Zeng, K. Li, Q.Y. Zhu, J.L. Wang, Y.N. Cao, S.J. Lu, Capture of CO_2 in carbon nanotube bundles supported with room-temperature ionic liquids: a molecular simulation study, Chem. Eng. Sci. 192 (2018) 94.

[19] B. Gurkan, F. Simeon, T.A. Hatton, Quinone reduction in ionic liquids for electrochemical CO_2 separation, ACS Sustain. Chem. Eng. 3 (2015) 1394.

[20] D. Bao, S. Ramu, A. Contreras, S. Upadhyayula, J.M. Vasquez, G. Beran, V.I. Vullev, Electrochemical reduction of quinones interfacing experiment and theory for defining effective radii of redox moieties, J. Phys. Chem. B. 114 (2010) 14467.

[21] J. Chen, B.K. Jin, Investigation on redox mechanism of 1,4-naphthoquinone by in situ FT-IR spectroelectrochemistry, J. Electroanal. Chem. 756 (2015) 36.

[22] B. Jin, J. Huang, A. Zhao, S. Zhang, Y. Tian, J. Yang, Direct evidence of hydrogen-bonding and/or protonation effect on p-benzoquinone electrochemical reduction by in situ IR spectroelectrochemical study, J. Electroanal. Chem. 650 (2010) 116.

[23] D. Li, L.J. Cheng, B.K. Jin, Investigation on PCET-accompanied dimerization of 5-hydroxy-1, 4-naphthoquinone in the process of electrochemical reduction by in situ FT-IR spectroelectrochemistry and density functional calculation, Electrochim. Acta 130 (2014) 387.

[24] M. Namazian, H.R. Zare, H. Yousofian-Varzaneh, Electrochemical behavior of tetrafluoro-p-benzoquinone at the presence of carbon dioxide: experimental and theoretical studies, Electrochim. Acta 196 (2016) 692.

[25] W. Yin, A. Grimaud, I. Azcarate, C.Z. Yang, J.M. Tarascon, Electrochemical reduction of CO_2 mediated by quinone derivatives: implication for Li-CO_2 battery, J. Phys. Chem. C 122 (2018) 6546.

[26] H. Cruz, I. Gallardo, G. Guirado, Understanding specific effects on the standard potential shifts of electrogenerated species in 1-butyl-3-methylimidazolium ionic liquids, Electrochim. Acta 53 (2008) 5968.

[27] N.V. Rees, R.G. Compton, Electrochemical CO_2 sequestration in ionic liquids; a perspective, Energy Environ. Sci. 4 (2011) 403.

[28] J.S. Wilkes, M.J. Zaworotko, Air and water stable 1-ethyl-3-methylimidazolium based ionic liquids, J. Chem. Soc. Chem. Commun. (1992) 965.

[29] B.K. Sweeny, D.G. Peters, Cyclic voltammetric study of the catalytic behavior of nickel(I) salen electrogenerated at a glassy carbon electrode in an ionic liquid (1-butyl-3-methylimidazolium tetrafluoroborate, $BMIM^+BF_4^-$), Electrochem. Commun. 3 (2001) 712.

[30] J. Howarth, Oxidation of aromatic aldehydes in the ionic liquid $bmimPF_6$, Tetrahedron Lett. 41 (2000) 6627.

[31] N. Hollingsworth, S.F.R. Taylor, M.T. Galante, J. Jacquemin, C. Longo, K.B. Holt, N.H. de Leeuw, C. Hardacre, CO_2 capture and electrochemical conversion using superbasic P-66614 - 124Triz, Faraday Discuss. 183 (2015) 389.

[32] M. Feroci, I. Chiarotto, G. Forte, S.V. Ciprioti, A. Inesi, Stability and CO_2 capture ability of electrogenerated N-heterocyclic carbene in parent 1-butyl-3-methylimidazoliun ionic liquid (BMIm-X): the role of X, Chemelectrochem 1 (2014) 1407.

[33] T. Benedetti, S. Naficy, A. Walker, D.L. Officer, G.G. Wallace, F. Dehghani, Solid-state poly(ionic liquid) gels for simultaneous CO_2 adsorption and electrochemical reduction, Energ. Technol. 6 (2018) 702.

[34] W.X. Cheng, B.K. Jin, P. Huang, L.J. Cheng, Y.P. Tian, Investigation on the π-dimer/σ-dimer of 1,8-dihydroxy-9,10-anthracenedione in the process of electrochemical reduction by using IR spectroelectrochemical cyclic voltabsorptometry and derivative cyclic voltabsorptometry, J. Phys. Chem. C 117 (2013) 3940.

[35] B.K. Jin, L. Li, J.L. Huang, S.Y. Zhang, Y.P. Tian, J.X. Yang, IR spectroelectrochemical cyclic voltabsorptometry and derivative cyclic voltabsorptometry, Anal. Chem. 81 (2009) 4476.

[36] X. Wang, B. Jin, X. Lin, In-situ FTIR spectroelectrochemical study of dopamine at a glassy carbon electrode in a neutral solution, Anal. Sci. 18 (2002) 931.

[37] A.D. Becke, Density-functional thermochemistry. III. The role of exact exchange, J. Chem. Phys. 98 (1993) 5648.

[38] M.J. Frisch, G.W. Trucks, H.B. Schlegel, G.E. Scuseria, M.A. Robb, J.R. Cheeseman, G. Scalmani, V. Barone, B. Mennucci, G.A. Petersson, H. Nakatsuji, M. Caricato, X. Li, H.P. Hratchian, A.F. Izmaylov, J. Bloino, G. Zheng, J.L. Sonnenberg, M. Hada, M. Ehara, K. Toyota, R. Fukuda, J. Hasegawa, M. Ishida, T. Nakajima, Y. Honda, O. Kitao, H. Nakai, T. Vreven, J.A. Montgomery Jr., J.E. Peralta, F. Ogliaro, M. Bearpark, J.J. Heyd, E. Brothers, K.N. Kudin, V.N. Staroverov, R. Kobayashi, J. Normand, K. Raghavachari, A. Rendell, J.C. Burant, S.S. Iyengar, J. Tomasi, M. Cossi, N. Rega, J.M. Millam, M. Klene, J.E. Knox, J.B. Cross, V. Bakken, C. Adamo, J. Jaramillo, R. Gomperts, R.E. Stratmann, O. Yazyev, A.J. Austin, R. Cammi, C. Pomelli, J.W. Ochterski, R.L. Martin, K. Morokuma, V.G. Zakrzewski, G.A. Voth, P. Salvador, J.J. Dannenberg, S. Dapprich, A.D. Daniels, O. Farkas, J.B. Foresman, J.V. Ortiz, J. Cioslowski, D.J. Fox, Gaussian 09, Revision B. 01, Gaussian, Inc., Wallingford CT, 2009.

[39] Y. Astuti, E. Topoglidis, P.B. Briscoe, A. Fantuzzi, G. Gilardi, J.R. Durrant, Proton-coupled electron transfer of flavodoxin immobilized on nanostructured tin dioxide electrodes: thermodynamics versus kinetics control of protein redox function, J. Am. Chem. Soc. 126 (2004) 8001.

[40] J. Safarov, C. Sperlich, A. Namazova, A. Aliyev, D. Tuma, A. Shahverdiyev, E. Hassel, Carbon dioxide solubility in 1-butyl-3-methylimidazolium tetrafluoroborate and 1-butyl-3-methylimidazolium tetrachloroferrate over an extended range of temperature and pressure, Fluid Phase Equilib. 467 (2018) 45.

[41] M.B. Shiflett, A. Yokozeki, Solubilities and diffusivities of carbon dioxide in ionic liquids: $bmimPF_6$ and $bmimBF_4$, Ind. Eng. Chem. Res. 44 (2005) 4453.

[42] L.X. Wu, H. Wang, Y. Xiao, Z.Y. Tu, B.B. Ding, J.X. Lu, Synthesis of dialkyl carbonates from CO_2 and alcohols via electrogenerated N-heterocyclic carbenes, Electrochem. Commun. 25 (2012) 116.

[43] J.H. Rheinhardt, P. Singh, P. Tarakeshwar, D.A. Buttry, Electrochemical capture and release of carbon dioxide, ACS Energy Lett. 2 (2017) 454.